Multiphase Integrated On-board Battery Chargers for Electrical Vehicles

I.Subotic, E.Levi, M.Jones
LIVERPOOL JOHN MOORES UNIVERSITY
School of Engineering, Byrom Street
Liverpool L3 3AF, UK
e-mail: I.Subotic@2011.ljmu.ac.uk

D.Graovac
INFINEON TECHNOLOGIES AG
Am Campeon 1-12
D-85579 Neubiberg
Germany
e-mail: Dusan.Graovac@infineon.com

Acknowledgement

The authors would like to acknowledge the Engineering and Physical Sciences Research Council (EPSRC) for supporting the Vehicle Electrical Systems Integration (VESI) project (EP/I038543/1).

Keywords

Multiphase drive, Battery charger, Electric vehicle.

Abstract

The paper considers on-board battery charging of electrical vehicles (EVs) using a multiphase voltage source and a multiphase propulsion motor. The multiphase inverter and the multiphase machine are fully integrated into the charging process. The proposed integrated on-board battery charger has an advantage of unity power factor operation with no torque production in the machine during the charging mode. The principle of the charging mode operation is based on the additional degrees of freedom that exist in multiphase machines. It is shown that they can be conveniently utilised to achieve charging through the machine's stator winding with zero electromagnetic torque. Detailed theoretical analysis is reported for a five-phase system, with a subsequent generalization to other multiphase systems with other higher odd numbers of phases. A mathematical model of a multiphase voltage source rectifier (VSR) is developed, its control in the charging mode is discussed, and the concept is validated by simulation.

Introduction

Fast battery chargers are mandatory for a wider use of EVs. There are two basic types of battery chargers, off-board and on-board, and for both types many configurations have been proposed [1]. However, only on-board chargers liberate their users from the need to search for charging stations, and allow them a freedom of charging their vehicles from almost any single-phase or three-phase (as appropriate) power socket. On-board battery chargers typically have, in addition to advantages, some drawbacks as well. If made like a separate unit, which is currently the case with many EVs, they increase the cost of the vehicle by introducing new power electronics elements. Depending on the model the additional cost can be up to $ 3,000 [2]. Their installation requires additional space and increases the weight. However, all these drawbacks can be overcome by integrating the existing propulsion motor and power electronics into the charging process [3]. An integrated charger was introduced for the first time in 1985 [4], and many various integrated solutions have been reported since [5].

A majority of EVs at present use a machine of induction type for propulsion [6], although permanent magnet synchronous machines are also a common choice. Nevertheless, currently only five integrated on-board solutions [7-11] allow fast (three-phase) charging incorporating these types of machines. In [7], during the charging mode, motor three-phase stator windings are in an open-end winding configuration. At one side they are connected to the three legs of the inverter, while the other three winding terminals at the other side are connected to a three-phase grid. Development of the rotating field occurs during the charging mode, so that the motor must be mechanically locked to avoid rotation, which presents a severe drawback. In [8], in order to provide a galvanic isolation, an induction machine

is used like a transformer in the battery charging mode. However, this solution increases the cost of the drive system since it requires a wound rotor, so that the isolation advantage is completely overshadowed. Another isolated solution is presented in [9]. It avoids the additional cost of wound rotor by having a stator with two sets of three-phase windings, which are shifted spatially by 30 degrees (split-phase or asymmetrical six-phase configuration). In the traction mode each pair of phases of the two three-phase windings that has spatial shift of 30 degrees is connected in series to constitute a single three-phase winding set. For the charging mode the system requires reconfiguration. The first set of three-phase windings is connected to the inverter on one side, and into the star on the other side, while the second set is connected into delta on one side, and to the grid at the other side. In contrast to the previous two, this one has an industrial potential.

A completely different charger topology is proposed in [10]. The solution uses mid-points of each of the three windings of a three-phase machine to connect them to a three-phase ac grid during charging (three-phase machine with accessible mid-points is in essence an equivalent of a symmetrical six-phase machine). Compared to the three previous configurations, this one has some distinct advantages: there is no torque production in the machine during charging mode; moreover, no hardware reconfiguration between propulsion and charging mode of operation is required and the solution is being considered for use in future EVs [12]. Another solution which does not require hardware reconfiguration is presented in [11]. The three phase grid connections are directly attached to the three isolated neutral points of a nine-phase machine. By simultaneous control of inverter legs belonging to the same winding set, the field is cancelled between these windings, and the torque production is avoided in the charging process. The last three configurations use multiphase machines. There is only one more proposal that uses a multiphase machine for charging operation [13]; however, it is applicable only for single-phase charging.

Multiphase drives are mainly used in high power applications. Their two main advantages over three-phase systems are reduced current (power) rating of the semiconductor switches and excellent fault-tolerant operation features [14]. In general, multiphase machines are characterised with existence of additional degrees of freedom with regard to the control. This brings in an added advantage over their three-phase counterparts in applications related to the integrated on-board charging of EVs, as will be shown in this paper. These additional degrees of freedom can be used for battery charging without any torque production. This paper for the first time considers multiphase supply as a fast charging option for EVs, and presents new multiphase integrated on-board chargers with unity power factor operation and the machine kept naturally at standstill during the charging process. The inverter and the machine are fully integrated into the charging process. The configurations employ phase-transposition rule [15] in order to ensure that the motor does not develop torque during charging, so that the machine naturally stays at standstill and its stator winding's leakage inductances are utilised for filtering during the charging process.

The paper is organized as follows. Detailed theoretical analysis is reported for a five-phase integrated charging system in the next section. A generalization is further made to all systems with odd numbers of phases higher than five in the subsequent section. This is followed by the mathematical model of a multiphase VSRs and the control algorithm for the proposed configurations. Finally, theoretical results are validated by simulations. The conclusions are given in the last section.

Theoretical analysis of a five-phase integrated charging system

At present on-board charging takes place with either single-phase or three-phase mains supply. In this paper it is assumed that the charging station is equipped with a multiphase supply system ($n > 3$) and this is a scenario that is currently futuristic but may become realistic some time in future. A multiphase supply in the charging station could be obtained in different ways. The simplest one would be based on a three-phase to *n*-phase transformer. Such transformer configurations are currently known for three-phase to five-phase transformers [16] and three-phase to seven-phase transformers [17]. The alternative solutions would be based on power electronic converters, and would require output voltage filtering. One could use either a three-phase to *n*-phase matrix converter [18, 19] or a back-to-back (two-stage)

converter with an *n*-phase inverter as the output stage. In what follows it is assumed that, whatever the source of the multiphase supply is, the voltages can be regarded as sinusoidal and symmetrical.

The first considered topology is a five-phase propulsion motor, which is star-connected with isolated neutral point in the normal driving cycle. For charging purposes the neutral point of the motor is opened and the phases are connected to the sinusoidal five-phase source. However, instead of connecting the motor phases *a* to *e* directly to *a* to *e* phases of the supply, the principle of phase transposition [15] is applied. The resulting connection diagram for the charging mode is as shown in Fig. 1. Parameters R_f and L_f in Fig. 1 in essence represent stator leakage impedance of the multiphase machine for all cases considered in the paper that are based on the phase transposition rule (the exception is the scheme of Fig. 2, considered shortly, where these parameters depend on the machine type). The basic idea here is that in a five-phase machine with sinusoidal spatial magneto-motive force distribution current flow according to Fig. 1 connection will not result in the rotating field (and hence there will be no torque developed), since the currents of the supply will map into the non-flux/torque producing plane [15]. Basically, the flux/torque producing $\alpha\beta$ plane will not be excited, as shown next.

Decoupling transformation matrix for a five-phase system is given with ($\alpha = 2\pi/5$)

$$[C]=\sqrt{\frac{2}{5}}\begin{matrix}\alpha\\ \beta\\ x\\ y\\ 0\end{matrix}\begin{bmatrix} 1 & \cos(2\pi/5) & \cos(4\pi/5) & \cos(6\pi/5) & \cos(8\pi/5)\\ 0 & \sin(2\pi/5) & \sin(4\pi/5) & \sin(6\pi/5) & \sin(8\pi/5)\\ 1 & \cos(4\pi/5) & \cos(8\pi/5) & \cos(12\pi/5) & \cos(16\pi/5)\\ 0 & \sin(4\pi/5) & \sin(8\pi/5) & \sin(12\pi/5) & \sin(16\pi/5)\\ 1/\sqrt{2} & 1/\sqrt{2} & 1/\sqrt{2} & 1/\sqrt{2} & 1/\sqrt{2}\end{bmatrix} \tag{1}$$

where power invariant form is used. For further considerations, it is convenient to combine the first two rows and the subsequent two rows into space vectors of the two planes, according to (*f* stands for any variable that is being transformed, e.g. current, voltage, etc.):

$$\begin{aligned}\underline{f}_{\alpha\beta} &= f_\alpha + jf_\beta = \sqrt{2/5}\left(f_a + \underline{a}f_b + \underline{a}^2 f_c + \underline{a}^3 f_d + \underline{a}^4 f_e\right)\\ \underline{f}_{xy} &= f_x + jf_y = \sqrt{2/5}\left(f_a + \underline{a}^2 f_b + \underline{a}^4 f_c + \underline{a}^6 f_d + \underline{a}^8 f_e\right)\end{aligned} \tag{2}$$

Here $\underline{a} = \exp(j\alpha) = \cos\alpha + j\sin\alpha$, where once more $\alpha = 2\pi/5$.

For the sake of simplicity, sinusoidal quantities *f* are taken further on as currents, and they are given as

$$i_{kg} = \sqrt{2}I\cos(\omega t - j2\pi/5) \qquad j = 0,1,2,3,4 \qquad k = a,b,c,d,e \tag{3}$$

where ω is the angular frequency of the supply and index *g* denotes the fictitious grid multiphase currents. Substitution of (3) into (2), while having in mind that due to the phase transposition machine currents are related to the grid currents according to (Fig. 1)

$$i_a = i_{ag} \qquad i_b = i_{cg} \qquad i_c = i_{eg} \qquad i_d = i_{bg} \qquad i_e = i_{dg} \tag{4}$$

leads to the following space vectors in the two planes of the five-phase system:

$$\underline{i}_{\alpha\beta} = 0 \qquad\qquad \underline{i}_{xy} = \sqrt{5}I\exp(j\omega t) \tag{5}$$

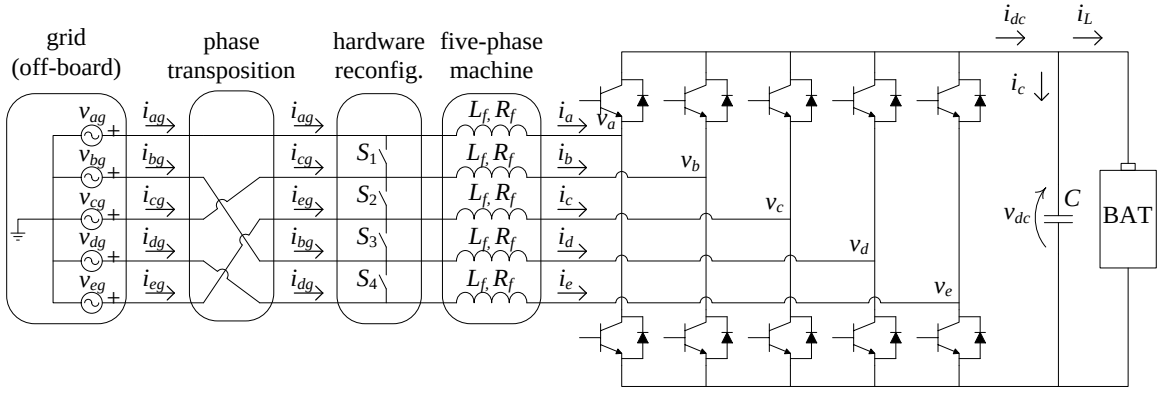

Fig. 1: Topology of the five-phase integrated on-board battery charger.

Hence it follows from (5) that the phase transposition connection of Fig. 1 maps grid phase currents into non-flux/torque producing (*xy*) plane of the machine, while the flux/torque producing currents ($\alpha\beta$) are identically equal to zero at all times. The machine will therefore develop zero average torque and will remain at standstill if connection of Fig. 1 is used, without any need for mechanical braking of the motor shaft. Zero-sequence component of (1) is identically equal to zero due to the assumed isolated star-connected five-phase grid.

An alternative connection, which does not follow the phase transposition rule, is shown in Fig. 2. It may be also, at least in theory, used. Such a connection produces pulsating field in the first plane, as shown next. The machine's *a* to *e* phases are now supplied with a phase sequence *a*, *c*, *b*, *e*, *d*. The space vectors (2) now become

$$\underline{i}_{\alpha\beta} = j2I\sin\omega t \qquad \underline{i}_{xy} = I(\sqrt{5}\cos\omega t - j\sin\omega t) \tag{6}$$

It follows from (6) that in the topology of Fig. 2 only one axis of the first plane is excited, so that a pulsating field is produced. In the second plane the components are now not of the same magnitude. However, since the second plane does not give torque production and the pulsating field in the first plane cannot produce an average torque, the machine again does not develop an average torque and hence stays at standstill during the charging process. Trajectories described with (6) in the two planes are illustrated in Fig. 3, taking the current rms value as equal to 1 per unit and grid frequency as 50 Hz.

Generalisation to systems with higher odd numbers of phases

Consider next a seven-phase machine. Only the situation with phase transposition is now considered, since it is believed to be better suited for potential real-world applications. The configurations for the charging mode are shown in Fig. 4. The difference, compared to the five-phase case, is that there are two *xy* planes rather than one (labelled with additional indices 1 and 2). Hence two connections to the grid are possible in charging mode. Once again, charging mode requires opening of the machine's neutral point and connection of motor phases to the grid phases, according to the schemes given in Fig. 4.

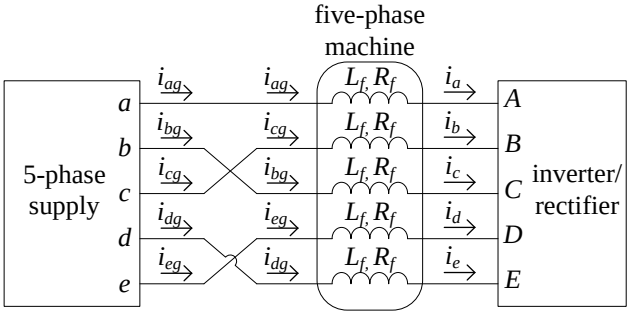

Fig. 2: An alternative five-phase system connection with zero average torque.

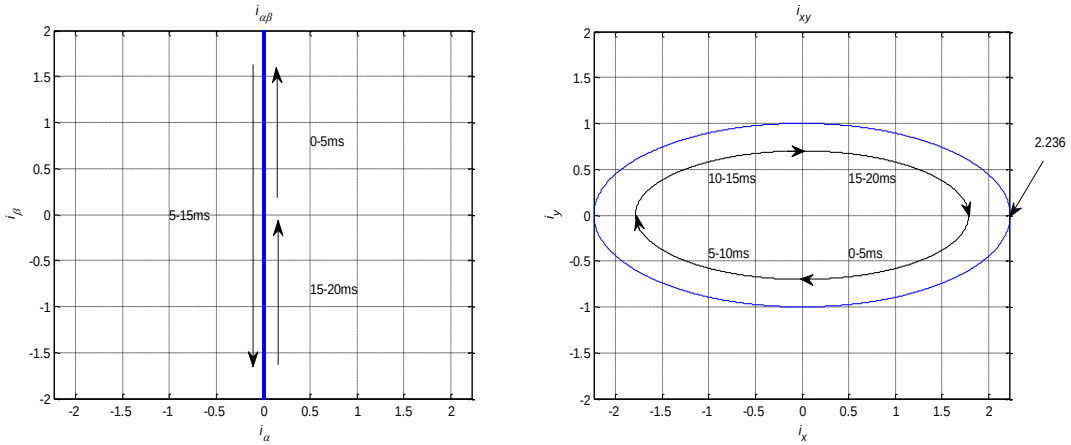

Fig. 3: Trajectories described with (6) in the charging mode of operation, according to the connection scheme in Fig. 2.

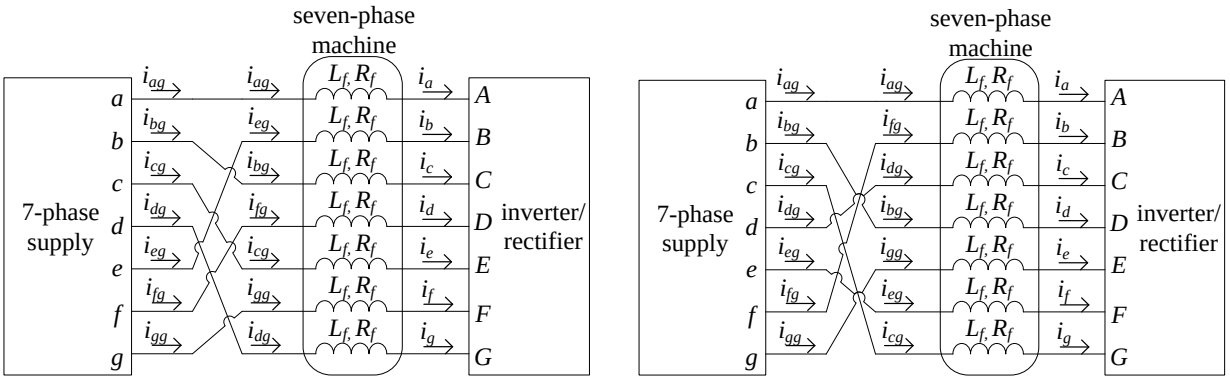

Fig. 4: Possible connections of a seven-phase machine to the seven-phase supply in charging mode.

The starting point is the general decoupling transformation matrix for a multiphase (*n*-phase) system [14], which is in the equivalent space vector representation, in the form of (2), now given with

$$\begin{aligned}
\underline{f}_{\alpha\beta} &= \sqrt{2/7}\left(f_a + \underline{a} f_b + \underline{a}^2 f_c + \underline{a}^3 f_d + \underline{a}^4 f_e + \underline{a}^5 f_f + \underline{a}^6 f_g\right) \\
\underline{f}_{x1y1} &= \sqrt{2/7}\left(f_a + \underline{a}^2 f_b + \underline{a}^4 f_c + \underline{a}^6 f_d + \underline{a}^8 f_e + \underline{a}^{10} f_f + \underline{a}^{12} f_g\right) \\
\underline{f}_{x2y2} &= \sqrt{2/7}\left(f_a + \underline{a}^3 f_b + \underline{a}^6 f_c + \underline{a}^9 f_d + \underline{a}^{12} f_e + \underline{a}^{15} f_f + \underline{a}^{18} f_g\right)
\end{aligned} \tag{7}$$

where $\underline{a} = \exp(j\alpha) = \cos\alpha + j\sin\alpha$ and $\alpha = 2\pi/7$. The grid currents are given with

$$i_{kg} = \sqrt{2} I \cos(\omega t - j2\pi/7) \qquad j = 0,1,..6 \qquad k = a,b,c,....f,g \tag{8}$$

For the connection diagrams of Fig. 4 the correlation between machine phase currents and grid currents is given with

$$i_a = i_{ag} \qquad i_b = i_{eg} \qquad i_c = i_{bg} \qquad i_d = i_{fg} \qquad i_e = i_{cg} \qquad i_f = i_{gg} \qquad i_g = i_{dg} \tag{9}$$

and

$$i_a = i_{ag} \qquad i_b = i_{fg} \qquad i_c = i_{dg} \qquad i_d = i_{bg} \qquad i_e = i_{gg} \qquad i_f = i_{eg} \qquad i_g = i_{cg} \tag{10}$$

respectively. Substitution of (9) into (7) gives the following space vectors for the first connection of Fig. 4:

$$\underline{i}_{\alpha\beta} = 0 \qquad \underline{i}_{x1y1} = 0 \qquad \underline{i}_{x2y2} = \sqrt{7} I \exp(-j\omega t) \tag{11}$$

On the other hand, for the second connection diagram in Fig. 4 the following space vectors are obtained:

$$\underline{i}_{\alpha\beta} = 0 \qquad \underline{i}_{x1y1} = \sqrt{7} I \exp(-j\omega t) \qquad \underline{i}_{x2y2} = 0 \tag{12}$$

As is obvious from (11) and (12), each of the two possible connection diagrams means that the charging process will utilise one of the two *xy* planes.

The procedure, illustrated here for a five-phase and a seven-phase machine, can be extended in the same manner to any other higher odd phase number by applying phase transposition according to the general connectivity matrix given in [15].

Modelling and control of multiphase voltage source rectifiers

Three-phase VSRs are widely used and their mathematical model is widely available [20]. The same is valid for the control related aspects. This however is not the case with multiphase VSRs, the main reason being the lack of real-world applications that demand this type of rectifier. With an increasing number of systems with multiphase inverters that might be used in automotive industry, multiphase VSRs are gaining in importance, mainly due to the fact that the same inverting hardware can be used also for rectification. With reference to Fig. 5 and its grid side, the following voltage equilibrium equation can be written:

$$[v_g] = [v_f] + [v] \tag{13}$$

where $[v_g]$ is the grid phase voltage matrix, $[v_f]$ is the matrix of voltage drops on the filter, and $[v]$ is the converter's phase voltage matrix. Voltage drops on the filter are equal to:

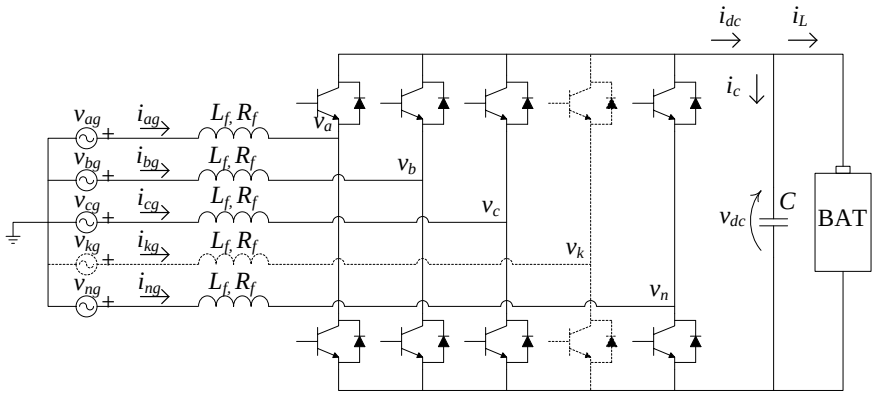

Fig. 5: Multiphase VSR system.

$$\left[v_f\right] = L_f \frac{d\left[i_g\right]}{dt} + R_f \left[i_g\right] \tag{14}$$

where $\left[i_g\right] = \left[i_{ag} \quad i_{bg} \quad i_{cg} \quad \ldots \quad i_{ng}\right]^T$, $L_f = L_{fa} = L_{fb} = \ldots = L_{fn}$, and $R_f = R_{fa} = R_{fb} = \ldots = R_{fn}$.
Converter phase voltages depend on the dc-bus voltage and switching states as follows:

$$\left[v\right] = v_{dc} \cdot \left(\left[s\right] - \frac{1}{n}\sum_{k=1}^{n} s_k \right) = v_{dc} \cdot \left(\left[I\right]_{n\times n} \left[s\right] - \frac{1}{n}\left[1\right]_{n\times n} \left[s\right] \right) = v_{dc} \cdot \left(\left[I\right]_{n\times n} - \frac{1}{n}\left[1\right]_{n\times n} \right)\left[s\right] \tag{15}$$

where $[I]_{nxn}$ is a unity matrix, $[1]_{nxn}$ is full matrix with all elements equal to one, and $[s]$ is the matrix of switching states. By substituting (14) and (15) into (13) one further has:

$$\left[v_g\right] = L_f \frac{d\left[i_g\right]}{dt} + R_f \left[i_g\right] + v_{dc} \cdot \left(\left[I\right]_{n\times n} - \frac{1}{n}\left[1\right]_{n\times n} \right)\left[s\right]. \tag{16}$$

By inspecting the right-hand part of Fig. 5, it can be seen that:

$$C\frac{dv_{dc}}{dt} = i_{dc} - i_L \tag{17}$$

where $i_{dc} = \left[s\right]^T \cdot \left[i_g\right]$. Hence:

$$C\frac{dv_{dc}}{dt} = \left[s\right]^T \cdot \left[i_g\right] - i_L \tag{18}$$

System model is given with (16) and (18). However, for control purposes the model has to be in the same reference frame in which current control is performed, i.e. synchronously rotating reference frame. It can be transformed by using at first the general decoupling transformation matrix for multiphase systems [14]; this is followed by application of the rotational transformation [D], which transforms only the first pair ($\alpha\beta$) of equations [14]. Upon transformations, (16) takes the form:

$$\begin{aligned} \left[v_{g(dq)}\right] = L_f \frac{d\left[i_{g(dq)}\right]}{dt} - L_f \begin{bmatrix} 0 & \omega_g & 0 & \ldots & 0 \\ -\omega_g & 0 & 0 & \cdots & 0 \\ 0 & 0 & 0 & \cdots & 0 \\ \vdots & \vdots & \vdots & \ddots & \vdots \\ 0 & 0 & 0 & \ldots & 0 \end{bmatrix} \cdot \left[i_{g(dq)}\right] + R_f \left[i_{g(dq)}\right] + \\ + v_{dc} \cdot \left(\left[I\right]_{n\times n} - \begin{bmatrix} & [0]_{(n-1)\times(n-1)} & & 0 \\ & & & \vdots \\ 0 & \cdots & & 1 \end{bmatrix}_{n\times n} \right)\left[s_{(dq)}\right] \end{aligned} \tag{19}$$

Equation (18) can be written in the rotating reference frame as:

$$\begin{aligned} C\frac{dv_{dc}}{dt} &= \left[s_{(\alpha\beta)}\right]^T \cdot \left(\left[D\right]^T \cdot \left[D\right] \cdot \left[i_{g(\alpha\beta)}\right]\right) - i_L = \left(\left[s_{(\alpha\beta)}\right]^T \cdot \left[D\right]^T\right) \cdot \left(\left[D\right] \cdot \left[i_{g(\alpha\beta)}\right]\right) - i_L = \\ &= \left(\left[D\right] \cdot \left[s_{(\alpha\beta)}\right]\right)^T \cdot \left(\left[D\right] \cdot \left[i_{g(\alpha\beta)}\right]\right) - i_L = \left[s_{(dq)}\right]^T \cdot \left[i_{g(dq)}\right] - i_L \end{aligned} \tag{20}$$

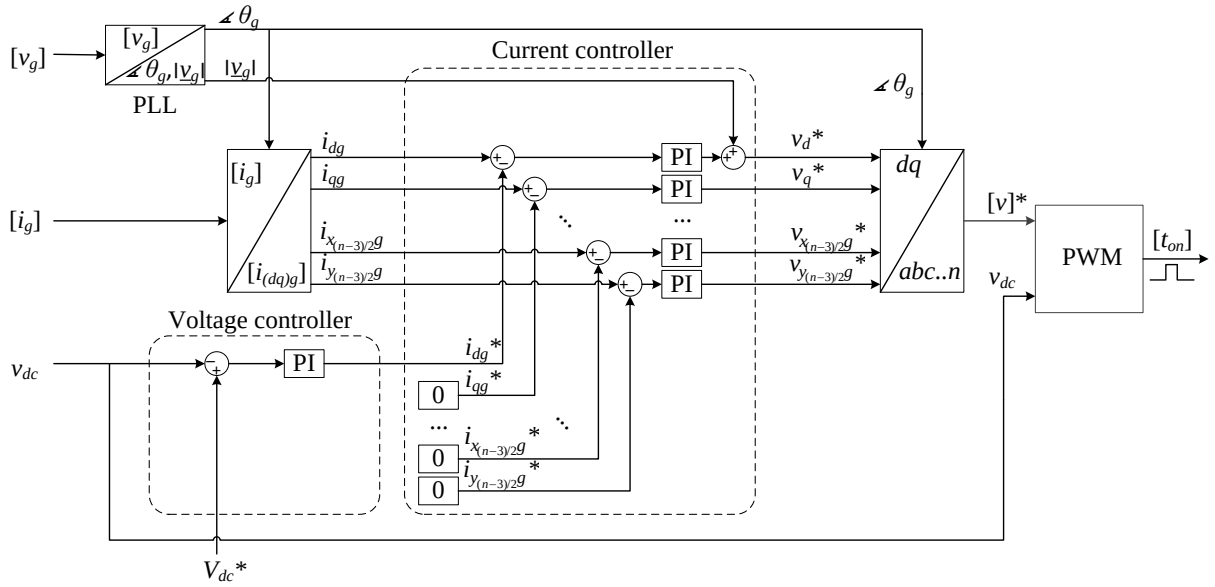

Fig. 6: Grid voltage oriented control (VOC) algorithm for multiphase systems.

The control algorithm for the system of Fig. 5 is given in Fig. 6. It should be noted that the current control requires a decoupling network which is not shown in Fig. 6 for the sake of simplicity. Grid voltages, grid currents, and dc voltage are measured.

For voltage oriented control (VOC) the information on the grid position is mandatory. Obtaining this information from measured grid voltages is commonly achieved by a phase locked loop (PLL). Once the grid voltage space vector position is known, it is possible to transform grid currents into the rotating (*dq*) reference frame that is grid-voltage oriented. This is necessary since the control goal is to achieve a unity power factor operation, which is best reflected in non-existence of the *q* grid current component in the grid-voltage oriented reference frame. When this is done, these *dq* currents represent real currents from which reference currents will be subtracted. The inverse sign in the controller comes from the fact that by increasing reference voltage, voltage that will be applied to the filter (machine windings) decreases. This is in contrast to the propulsion mode of operation.

All reference current components are zero, except for the *d* component. There are two ways of obtaining the *d* component of the current reference, which match two charging modes demanded by the battery. The most conventional way of charging the battery is CC-CV (constant current-constant voltage) method. It consists of charging the battery with a constant current, equal to the maximum charging current, up to the instant when voltage reaches a certain cut-off level. From that point on the battery gets charged from the constant voltage source until the current drops below the value of 10% of the maximum current, which represents the end of the charging process. Thus obtained *d* component of the reference current for CV mode is actually the output of the PI dc voltage controller (Fig. 6). When current reference is obtained, it represents the final signal that enters the current controller.

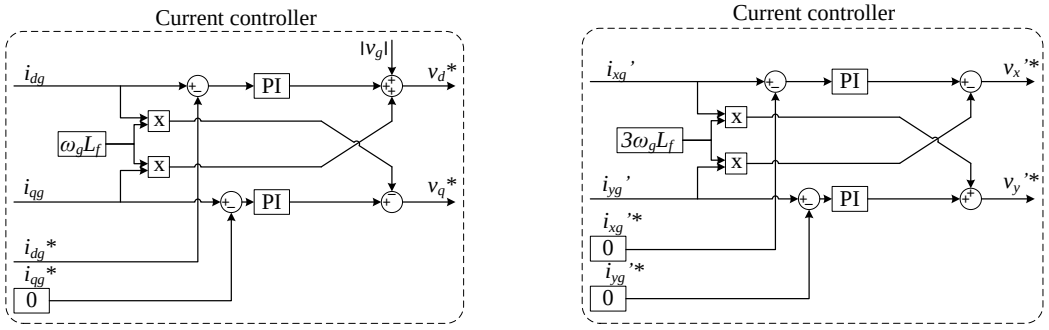

Fig. 7: Decoupling network: in the *dq* plane (left), optional for the *xy* plane (right).

In three-phase rectifiers current control is executed only in the *dq* plane. From (19) it can be seen that there are coupling terms in the *dq* voltage equations, proportional to $\pm\omega_g L_f$. Hence a decoupling network is needed (the left part of Fig. 7). However, multiphase rectifiers require current control in other planes as well (Fig. 6). This can be done in a number of ways. One possibility is depicted for the five-phase case in Fig. 7 on the right-hand side. Current *xy* components are also transformed rotationally (in contrast to (19)), into a reference frame that rotates in anti-synchronous direction at the speed of $3\omega_g$. Current *xy* components in this rotating reference frame are denoted as *x'y'* components. This means that the third current harmonic, caused by the existence of the inverter dead time, will appear in this reference frame as a dc quantity. In this case a decoupling network is necessary also in the second plane and it is shown in the right part of Fig. 7. The decoupling terms now have inverse signs.

The PWM block in Fig. 6 corresponds to a simple carrier-based PWM with zero-sequence injection. In the propulsion mode of operation the multiphase drive is operated according to the well known rotor field oriented control principles for multiphase machines [21].

Simulation results

A simulation of the charging mode of operation of a five-phase system is executed in Matlab/SymPowerSystems software package in order to provide verification of the theoretical results presented in the paper. Grid phase voltage has rms value of 240V and 50Hz frequency. For the battery representation a single resistor R_L=0.5Ω in conjunction with an ideal voltage source E=647V is utilized. Converter switching frequency is 2kHz and the dead time is 6μs. The dc-bus capacitance is C_{dc} = 1.5mF. The 50Hz five-phase induction machine parameters are: $R_s = R_r$ = 3Ω, $L_{\gamma s} = L_{\gamma r}$ = 45mH, L_m = 0.515H, two pole pairs, J = 0.1kgm^2. The grid phase voltage is an input into the simulation and it is taken as being perfectly sinusoidal.

For simplicity, simulation is performed only in the continuous voltage (CV) mode with the dc-bus voltage reference value of 650V. Fig. 8a presents the grid phase voltage and current. The current at the same time represents the machine phase current (its current components are given in Fig. 9), since the grid currents are the same as machine phase currents, except for the different phase order. Grid phase current follows the shape of the voltage, with a switching ripple that is not uniform during the period due to a fixed switching frequency. It can be seen that the current is in phase with the grid voltage, which confirms unity power factor operation during charging. The grid phase current spectrum is given in Fig. 8b and it contains only small values of low order harmonics. The third harmonic is almost completely removed with the current control in the second plane (right part of Fig. 7), and the only noticeable harmonic is the 7th, which is also caused by the dead-time effect. As the grid is five-phase, there are also the additional *xy* current components. These are depicted in the reference frame used for their control (anti-synchronous, rotating at $3\omega_g$; i_x' and i_y' are illustrated), together with the *dq* current components in the synchronous reference frame in Fig. 8c. It can be seen that the *q*, *x* and *y* components are kept at zero during the whole charging period, while only the *d* component has a non-zero value, since it is used for the power transfer from the grid into the battery. Considering that the rotational transformation is grid-voltage oriented, this also means that the charging is with the unity power factor.

Fig. 9 shows current components in the machine. From Fig. 9a it can be seen that currents in the torque producing ($\alpha\beta$) plane are controlled to zero with only a switching ripple, which was the initial goal during the charging process. Fig. 9b shows *xy* current components. Clearly, these current components in the machine correspond to the *dq* (i.e. $\alpha\beta$) components of the grid currents. Hence, during the charging process, currents are completely transferred from the torque producing ($\alpha\beta$) to the non-torque producing (*xy*) plane, which is in accordance with the theoretical results of (5).

Converter phase voltage and its spectrum are shown in Fig. 10. The third harmonic that is generated by the dead time is almost completely compensated, and the phase voltage has a very small dead-time induced 7th harmonic. Fig. 11a shows the machine's torque and speed and these are both obviously kept at zero, so that the rotor naturally stays at standstill during the battery charging. Finally, the dc-bus

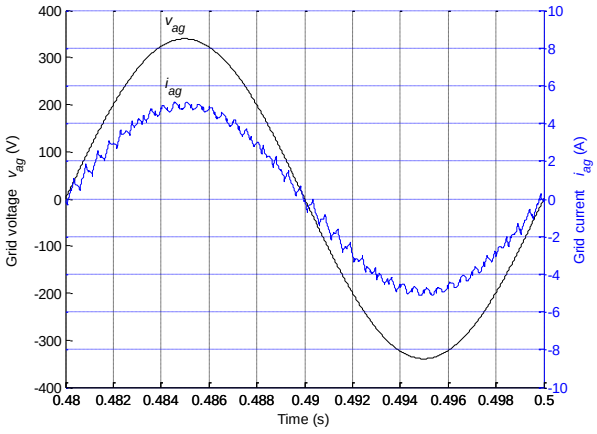

a)

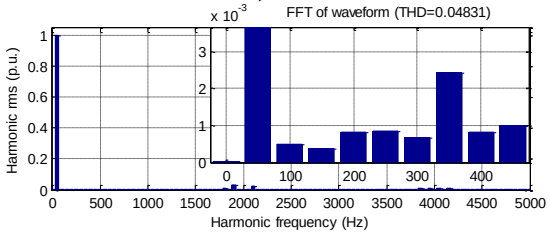

b)

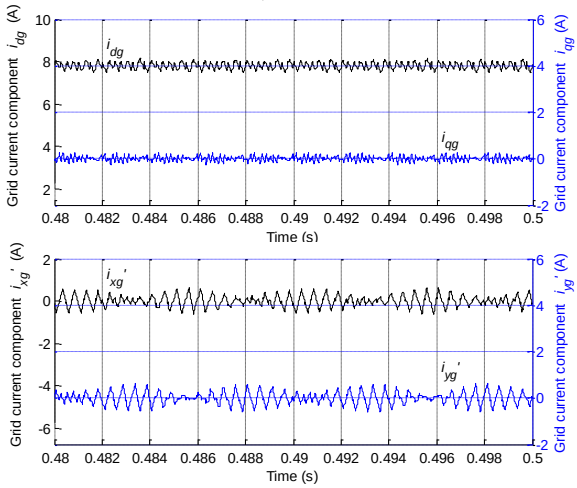

c)

Fig. 8: Grid: (a) phase voltage and current, (b) current spectrum, (c) current components.

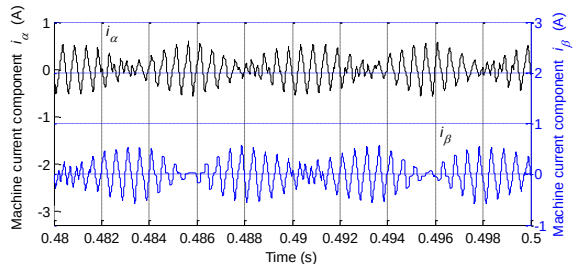

a)

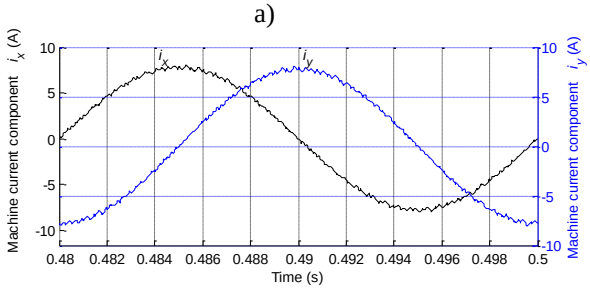

b)

Fig. 9: Machine current components: (a) i_α and i_β, (b), i_x and i_y.

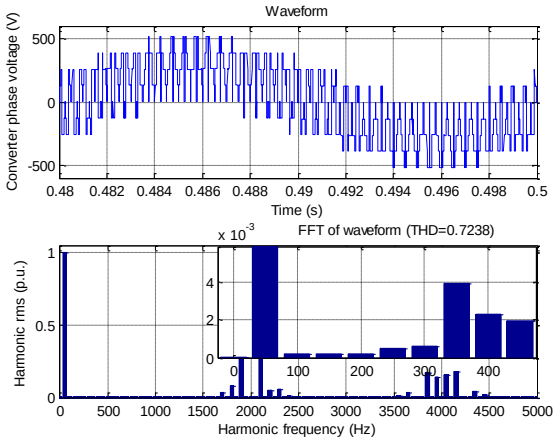

Fig. 10: Converter phase voltage and its FFT.

voltage and the battery charging current are shown in Fig. 11b. Dc-bus voltage is kept at 650V without steady state error, and the charging current is of the same shape as the battery is represented only with a constant voltage source and a resistor.

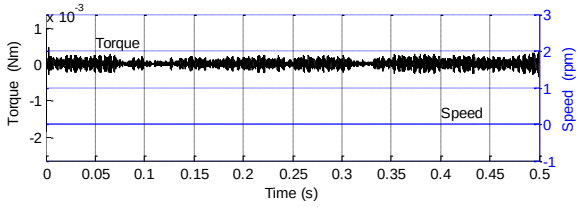

a)

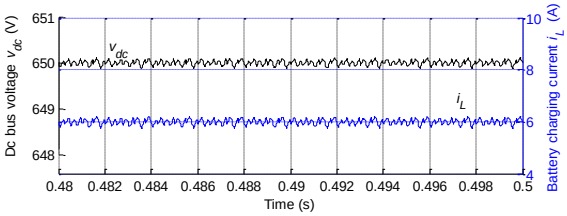

b)

Fig. 11: (a) Machine torque and rotor speed; (b) Dc-bus voltage and charging current.

Conclusion

The paper analyses means for charging an EV's battery from a multiphase source, using the principle of phase transposition in connection of the grid to the machine's windings. It proposes new integrated on-

board charging configurations incorporating an inverter and propulsion machine into the charging process. A complete mathematical model of a multiphase voltage source rectifier (VSR) is developed, and its control in the charging mode is discussed. Simulation of the five-phase configuration demonstrates feasibility of charging with unity power factor, with zero torque production in the machine.

References

[1] M. Yilmaz and P.T. Krein, "Review of battery charger topologies, charging power levels and infrastructure for plug-in electric and hybrid vehicles," *IEEE Trans. on Power Elec.*, vol. 28, no. 5, pp. 2151 – 2169, 2013.

[2] "Tesla Roadster specifications," http://www.teslamotors.com/display_data/teslaroadster_specsheet.pdf, 2009.

[3] S. Haghbin, S. Lundmark, M. Alakula, and O. Carlson, "Grid-connected integrated battery chargers in vehicle applications: review and new solution," *IEEE Trans. on Ind. Elec.*, vol. 60, no. 2, pp. 459-473, 2013.

[4] J.M. Slicker, "Pulse width modulation inverter with battery charger," *US Patent* 4,491,768, 1985.

[5] M. Bertuoluzzo, N. Zabihi, and G. Buja, "Overview on battery chargers for plug-in electric vehicles," *Int. Power Electronics and Motion Control Conf. EPE-PEMC ECCE Europe*, Novi Sad, Serbia, CD-ROM, 2012.

[6] J. de Santiago, H. Bernhoff, B. Ekergård, S. Eriksson, S. Ferhatovic, R. Waters, and M. Leijon, "Electrical motor drivelines in commercial all-electric vehicles: A review," *IEEE Trans. on Vehicular Technology*, vol. 61, no. 2, pp. 475-484, 2012.

[7] S. Kinoshita, "Electric system of electric vehicle," *US Patent* No. 5,629,603, 1997.

[8] F. Lacressonniere and B. Cassoret, "Converter used as a battery charger and a motor speed controller in an industrial truck," *Proc. Eur. Conf. on Power Elec. and Appl. EPE*, Dresden, Germany, CD-ROM, 2005.

[9] S. Haghbin, S. Lundmark, M. Alakula, and O. Carlson, "An isolated high-power integrated charger in electrified-vehicle applications," *IEEE Trans. on Vehicular Technology*, vol. 60, no. 9, pp. 4115-4126, 2011.

[10] L. De Sousa, B. Silvestre, and B. Bouchez, "A combined multiphase electric drive and fast battery charger for electric vehicles," *Proc. IEEE Vehicle Power and Propulsion Conf. VPPC*, Lille, France, CD-ROM, 2010.

[11] I. Subotic, E. Levi, M. Jones, and D. Graovac. "On-board integrated battery chargers for electric vehicles using nine-phase machines," *IEEE Int. Electric Machines and Drives Conf. IEMDC*, Chicago, IL, 2013.

[12] A. Sandulescu, F. Meinguet, X. Kestelyn, E. Semail, and A. Bruyere, "Flux-weakening operation of open-end winding drive integrating a cost-effective high-power charger," *IET Electr. Syst. in Transportation* (to appear), 2013.

[13] S. Haghbin, T. Thiringer, and O. Carlson, "An integrated split-phase dual-inverter permanent magnet motor drive and battery charger for grid-connected electric or hybrid vehicles," *Int. Conf. on Electrical Machines ICEM*, Marseille, France, pp. 1941-1947, 2012.

[14] E. Levi, R. Bojoi, F. Profumo, H.A. Toliyat, and S. Williamson, "Multiphase induction motor drives - a technology status review," *IET Elect. Power Appl.*, vol. 1, no. 4, pp. 489-516, 2007.

[15] E. Levi, M. Jones, S.N. Vukosavic, and H.A. Toliyat, "A novel concept of a multiphase, multimotor vector controlled drive system supplied from a single voltage source inverter," *IEEE Trans. on Power Electr.*, vol. 19, no. 2, pp. 320- 335, 2004.

[16] A. Iqbal, S. Moinuddin, M.R. Khan, S.M. Ahmed, and H. Abu-Rub, "A novel three-phase to five-phase transformation using a special transformer connection," *IEEE Trans. on Power Delivery*, vol. 25, no. 3, pp. 1637-1644, 2010.

[17] S. Moinoddin, A. Iqbal, H. Abu-Rub, M.R. Khan, and S.M. Ahmed, "Three-phase to seven-phase power converting transformer," *IEEE Trans. on Energy Conversion*, vol. 27, no. 3, pp. 757-766, 2012.

[18] S.M. Ahmed, A. Iqbal, and H. Abu-Rub, "Generalized duty-ratio-based pulsewidth modulation technique for a three-to-*k* phase matrix converter," *IEEE Trans. on Ind. Electr.*, vol. 58, no. 9, pp. 3925-3937, 2011.

[19] A. Iqbal, S.M. Ahmed, and H. Abu-Rub, "Space vector PWM technique for a three-to-five-phase matrix converter," *IEEE Trans. on Ind. Appl.*, vol. 48, no. 2, pp. 697-707, 2012.

[20] M. Jasinski and M.P. Kazmierkowski, "Fundamentals of ac-dc-ac converters control and applications," in *The Industrial Electronics Handbook – Power Electronics and Motor Drives* (Chapter 16), edited by B.M. Willamowski and J.D. Irwin, CRC Press, 2011.

[21] E. Levi, "FOC: Field oriented control," in *The Industrial Electronics Handbook – Power Electronics and Motor Drives* (Chapter 24), edited by B.M. Willamowski and J.D. Irwin, CRC Press, 2011.